Effect of a fluid-wall interaction on a drying layer

Alla Oleinikova and Ivan Brovchenko*
Physical Chemistry, University of Dortmund, Otto-Hahn-Str. 6, Dortmund, D-44227, Germany
(Received 14 April 2007; published 18 October 2007)

Density profiles of Lennard-Jones liquid confined in slit pore with weakly attractive or hard walls are studied along the pore coexistence curve. In the large pores, the thickness L_0 of a drying layer increases approximately as the bulk correlation length ξ_- when approaching the bulk critical temperature T_c. Strengthening of the fluid-wall interaction suppresses the thickness of a drying layer and yields a logarithmic growth of L_0 with $\tau=1-T/T_c$. Existence of the two distinct regimes in the temperature behavior of L_0 may reflect a partial drying transition expected for the weak long-range fluid-wall interactions. Confinement in small pores suppresses strongly the drying layer and its thickness grows as $\sim\ln(\tau)$ upon heating with subsequent saturation. The sharpness of the interface between a liquid and a drying layer is studied in dependence on the fluid-wall interaction and pore width.

DOI: 10.1103/PhysRevE.76.041603 PACS number(s): 68.08.Bc, 05.70.Jk, 64.70.Fx

I. INTRODUCTION

Characterization of the fluid properties near a solid surface is important in various fields of science and technology. Local properties of a fluid near the surface determine character of its flow in channels, long-range attraction (repulsion) between two surfaces in liquid, affect conformation of biomolecules, etc. Analysis of the local properties of a fluid requires the knowledge of the density distribution near the surface. For various applications, it is necessary to describe the local fluid density by an analytical function of a distance to the wall. Density profiles of a fluid near the surface are determined, first of all, by the fluid-wall interaction and by the location of the considered thermodynamic state with respect to the liquid-vapor phase transition and its critical point. A situation, when liquid near the surface coexists with saturated vapor, is of the most practical importance.

At the liquid-vapor coexistence curve one of the coexisting phase may undergo wetting (drying) transition at some temperature below the bulk critical temperature T_c [1–4]. Near a strongly attractive surface, a macroscopically thick (infinite) layer of a liquid phase separates a vapor phase from the surface above the temperature T_w of a wetting transition. In the case of a weak fluid-wall interaction, the drying transition, that is appearance of a macroscopic vapor layer between the surface and liquid phase, is expected with approaching the drying transition temperature. The thickness of a wetting or drying layer is one of the key parameters necessary for the description of the fluid density profiles near a surface.

Due to the strong asymmetry of liquid and vapor phases, the wetting and drying transitions of fluids are rather different phenomena. However, they share many common features with a wetting transition in the Ising model, where two coexisting phases are completely symmetrical. Surface phase diagram of the Ising model in the presence of a short-range surface field, which acts on spins in the surface layer only, was proposed by Nakanishi and Fisher [3]. In the case relevant for fluid, when interaction between spins does not change noticeably near the surface, the wetting transition is of the first order for strong surface fields and turns to the second order for the weak surface fields, when T_w is close to T_c. In the case of a second-order or critical wetting, the thickness L_0 of a wetting layer grows continuously to infinity, when approaching T_w from lower temperatures. At zero bulk field (equivalent to the coexistence curve of a fluid), L_0 diverges logarithmically within mean field approximation [5]

$$L_0 \approx \xi_- \ln \frac{T_w}{T_w - T}, \tag{1}$$

where ξ_- is the bulk correlation length at the coexistence curve, which diverges as $\tau^{-\nu}$ with $\tau=(T_c-T)/T_c$ and $\nu \approx 0.63$. The logarithmic divergence [Eq. (1)] remains intact when fluctuations are accounted for within renormalization group analysis [6].

The wetting temperature, order of the wetting transition, fluctuation regime are strongly sensitive to the details of the fluid-fluid and fluid-wall interactions and to their range in particular [5,7–14]. In the case of a long-range fluid-fluid interaction, the thickness of a wetting layer shows strong divergence approaching the temperature of the critical wetting transition [8,15]:

$$L_0 \approx (T_w - T)^{-1}. \tag{2}$$

For fluids with short-range interactions, the wetting properties are determined by the decay range of a fluid-wall potential U_w. Whereas for the short-range fluid-wall interactions, both first-order and second-order wetting transitions are possible [3], only first-order wetting is expected for the long-range fluid-wall potential [10,11,14].

Competition between short-range and long-range fluid-wall forces may prevent the wetting transition, if these two potentials favor different phases. In this case, the interface between the wetting layer and nonwetting phase will be attracted to the surface and infinite wetting layer may appear at the bulk critical point only [9]. Below T_c, there is a partial

*brov@pc2a.chemie.uni-dortmund.de

wetting layer, whose thickness L_0 may be large but remains finite at $T<T_c$ and diverges as a bulk correlation length ξ_- upon approaching the critical point [9]:

$$L_0 \sim \xi_-. \tag{3}$$

This case is also relevant for the drying transition, which occurs in a liquid phase near the wall, interacting with fluid molecules via a long-range potential (for example, via van der Waals forces). When the short-range part of this potential favors drying, its long-range tail ultimately attracts liquid-vapor interface to the wall. As a result, the drying transition in the case of long-range fluid-wall interactions occurs at the critical point only [9–11,16]. Accordingly, the thickness of a drying layer should diverge as a bulk correlation length when approaching T_c [Eq. (3)]. If the fluid-wall attraction does not exceed some threshold value, a first-order partial drying transition between thin and thick drying layers may occur at some temperature below T_c [10,11]. The temperature of this transition decreases upon weakening the fluid-wall interaction [11]. Note, that close to T_c, the thickness of a drying layer should follow Eq. (3) both in the presence or absence of the partial drying transition [9,10].

Since long-range dispersion interactions between solid substrate and fluid molecules are unavoidable in real systems, the formation of a macroscopic vapor layer between the liquid and the surface is not possible. Indeed, a drying transition was never observed experimentally [17,18]. However, occurrence of a drying transition at the bulk critical temperature assumes the appearance of a microscopic drying layer below T_c. The experimental studies indicate depletion of liquid density near weakly attractive surfaces [17,19–23]. This depletion may be caused by the existence of a drying layer and respective liquid-vapor interface near the surface. Alternatively, liquid density depletion may originate from the missing-neighbor effect, which modifies the critical behavior near the boundary [24] and causes exponential decay of liquid density toward the surface [25,26].

The available experimental techniques give very rough estimation of the liquid density profiles near the surfaces. In particular, liquid density depletion is typically described by the two-box model, which imposes existence of a fluid layer near the surface with some uniform low density, whereas beyond this layer there is a constant density liquid. In the near future, quantitative characterization of the fluid density profiles by experimental methods seems to be problematic. In such situation, computer simulations is the main source of "experimental" data, which gives the details of fluid properties near various surfaces in a wide range of thermodynamic states. In simulations, the properties of a fluid near a planar surface can be studied in the slit pore geometry only. Liquid-vapor coexistence of fluids confined in pores occurs at different chemical potential than the bulk coexistence. The shift of the phase transition depends on the pore size and on the fluid-wall interaction [27–29]. The temperature dependence of this shift is unknown in the general case. As confinement in pores may strongly affect fluid density profiles, the meaningful results for semi-infinite system may be obtained by studies of fluid confined in pores of various sizes.

Thickness of a drying layer was studied theoretically mainly for two thermodynamic paths: along isotherms with approaching the liquid-vapor coexistence and along the liquid-vapor coexistence curve. In both cases, the study of the wetting phenomena requires knowledge of the liquid-vapor coexistence curve. The systems with long-range fluid-wall interaction are of the main interest due to their similarity with typical fluid-wall interaction in nature. Studies of less realistic systems with short-range fluid-wall interaction (including a hard wall) should help to test the limiting behavior with decreasing strength and range of the fluid-wall interaction.

A planar hard wall is completely dry (i.e., a macroscopic vapor layer separates a liquid phase from a wall) for all temperatures, where liquid-vapor coexistence occurs in a semi-infinite system [30]. Out of the bulk coexistence, the thickness L_0 of a drying layer is finite and it is controlled by the shift of the chemical potential $\delta\mu$ relatively to the bulk coexistence. In the particular case of fluids with short-range interparticle potential, such as a truncated Lennard-Jones (LJ) fluid, the thickness of a vapor layer near a hard wall depends on $\delta\mu$ as [31]

$$L_0 = \xi \ln \frac{a}{(\rho_l - \rho_v)\delta\mu}, \tag{4}$$

where ρ_l and ρ_v are the densities of the liquid and vapor phases far from the interface, respectively, ξ is the decay length of the vapor tail of the liquid-vapor interface, that is correlation length ξ_- of the bulk vapor, and $a>0$ is a system dependent parameter. Density profiles of various fluids near a hard wall were studied extensively using density functional approach and by computer simulations (see, for example, Refs. [32–38]). Most of the simulations (for rare exclusion, see Ref. [37]) were performed for the thermodynamics states out of the liquid-vapor coexistence.

The drying transition near attractive surfaces was studied mostly for the short-range fluid-wall interaction: For the square-well fluid near a square-well wall [34,39–41] and for the LJ fluid, interacting via cutted LJ potential with a wall [16,42–48]. A liquid-wall contact angle, calculated at some given temperature for various strengths of the fluid-wall interaction, yields estimation of the threshold strength, which enables a drying transition. Such analysis was performed for one temperature for the LJ fluid and for five temperatures for the square-well fluid. Increasing of the range of the fluid-wall attraction [16] suppressed the drying transition in accordance with theoretical expectations [9–11]. To our knowledge, evolution of the thickness L_0 of a drying layer near a weakly attractive or hard wall with approaching the bulk coexistence at constant temperature or along the liquid-vapor coexistence with approaching T_c was never studied by computer simulations. This does not allow a test of the theoretical expectations and complicates attempts to describe a liquid density profiles in the presence of a drying layer in a universal way.

To study the drying or wetting transition, the liquid-vapor coexistence should be approached or established in the simulated system. Typically, liquid-vapor equilibrium was achieved by simulations in a constant-volume ensemble with

a fluid, confined in slit pores with symmetrical walls or asymmetrical walls (one attractive wall and one hard wall) [16,34,39–48]. The average density of the confined fluid was fixed at some value deeply inside the two-phase region, that results in a phase separation inside the pore. As the lateral size of this pore was close to its width, one or two liquid-vapor interface(s) develops parallel to the walls and the wetting (drying) phase is represented by one or two wetting (drying) layer(s) only. Of course, the correct reproduction of the liquid-vapor coexistence and description of a wetting (drying) layer in such simulation systems is questionable. The problem may be solved by noticeable increase of the lateral pore size, that provides two coexisting phases with liquid-vapor interface normal to the walls. However, currently this can be done for small pores only.

The liquid-vapor coexistence of confined fluid can be calculated more accurately, when the interface between two coexisting phases (which should be not mixed with the presence of a wetting or drying layer) does not appear in the system simulated. This can be done, for example, by simulations in the grand canonical or in the Gibbs ensemble. This makes possible studies of the liquid-vapor coexistence curve of fluids in pores of various sizes, with subsequent extrapolation of the results to semi-infinite systems. We used this approach in the simulation studies of the surface phase transitions and surface critical behavior of LJ fluid [26,49–52] and water [25,51–54]. In particular, we have found [49] that the thickness of a drying layer L_0 seems to be governed by the bulk correlation length ξ_- at low temperatures but it grows much slower than ξ_- when approaching the critical temperature. It was not clear whether this behavior of L_0 is caused by confinement or by relatively strong fluid-wall interaction.

In the present paper, we study evolution of the liquid density profiles along the liquid-vapor coexistence curve of LJ fluid confined in slit pores with hard and weakly attractive walls. We test the possibility to describe the liquid density profiles in universal way with minimal number of system dependent parameters. This assumes knowledge of the thickness L_0 of a drying layer and its temperature dependence along the bulk and pore liquid-vapor coexistence curves. We examine a possibility to describe the sharpness of the interface between liquid phase and drying layer using the bulk correlation length. To clarify the effect of confinement, simulations were performed in the pores of 40 and 12σ width. The effect of the strength of a fluid-wall interaction on the temperature evolution of the liquid density profiles is studied in the range of interactions relevant for the case of a liquid water near paraffinlike and more hydrophobic surfaces.

II. METHODS

We studied LJ fluid, having an interparticle interaction of the form:

$$U_{\mathrm{LJ}}(r) = 4\epsilon[(\sigma/r)^{12} - (\sigma/r)^{6}], \tag{5}$$

where ϵ measures the well depth of the potential, while σ sets the length scale. The potential was spherically truncated at a radius 2.5σ and left unshifted. No long-range corrections were applied to account for effects of the truncation. The bulk liquid-vapor coexistence curve of this LJ fluid was studied in detail and its critical point was accurately located [26,55]. The LJ fluid was confined in the slit pores of width H with structureless walls. The hard wall potential was modeled as

$$U_h = \infty, \quad z \leqslant 0 \quad \text{or } z \geqslant H,$$

$$U_h = 0, \quad 0 < z < H, \tag{6}$$

where z measures the distance of the center of LJ molecule to the hard wall. The attractive walls interact with the LJ fluid via the long-range potential of a single plane of LJ molecules:

$$U_w(z) = 4\epsilon f[0.4(\sigma/z)^{10} - (\sigma/z)^4], \tag{7}$$

where parameter f determines the strength of the fluid-wall interaction relatively to fluid-fluid interaction. No truncation was applied to $U_w(z)$. The distance z in Eq. (7) is not a fully appropriate measure of the distance of molecules to the attractive surface, since part of this distance is not accessible for the centers of molecules. A more reasonable measure of the distance of molecules to the surface is $\Delta z = z - 0.55\sigma$ (see [25,26,49,50] for more details). Accordingly, the volume accessible for the centers of molecules in the pores with weakly attractive walls is reduced with respect to the pores with hard walls by a factor of about 1.03 for $H = 40\sigma$ and 1.10 for $H = 12\sigma$.

In the present paper, we report the simulation results obtained for large ($H = 40\sigma$) and small ($H = 12\sigma$) pores with hard walls and large pores ($H = 40\sigma$) with extremely weakly attractive walls [$f = 0.1$ in Eq. (7)]. The well depth of this fluid-wall potential is about 25% of the well depth of the fluid-fluid potential. At some temperatures, the liquid-vapor coexistence was simulated in the pore with more attractive walls ($f = 0.4$). Besides, simulation results for LJ fluid in pores ($H = 12\sigma$ and 40σ) with $f = 0.3$ [49] were used in the data analysis.

Liquid-vapor coexistence curves of the confined LJ fluid were determined using Monte Carlo (MC) simulations in the Gibbs ensemble (GEMC) [56]. In the GEMC, two coexisting phases are represented by fluid in two simulation cells. The chosen temperature is kept equal in both cells, equality of the chemical potential is achieved by molecular transfers between the cells and equality of pressure is provided by random changes of the cell volumes, keeping the total volume of two cells to be constant. The acceptance probability of molecular transfers between the cells varied from 0.5% at low temperatures to about 10% at high temperatures. The number of successful transfers between the coexisting phases per particle varied from dozens at low temperatures to several hundreds at high temperatures. The maximal variation of the volume was about 0.5 to 1.5%, providing an acceptance probability of this move from 10 to 30%. In the course of the GEMC simulations, conventional MC moves, molecular transfers and volume changes were performed randomly with the probabilities ~75%, ~25%, and <1%, respectively. The typical overall length of a simulation run was $\sim 10^8$ MC steps. The total number of molecules in the liquid and vapor

phases was about 8000 for the pores with $H=40\sigma$ and about 2000 for the pores with $H=12\sigma$. The lateral size of the simulated cells with a liquid phase was about 17σ and 20σ for the pores with $H=12\sigma$ and 40σ, respectively. To test the effect of the finite system size on the possible appearance of capillary waves near pore walls, we have simulated free liquid-vapor interface of the same LJ fluid at several temperatures. In these constant-volume simulations, the lateral system size (20σ) and number of molecules in the system (10000) were close to the corresponding parameters in the simulations of LJ fluid in pores with $H=40\sigma$. More details of the simulations, parameters of the model fluid, as well as its bulk coexistence curve are given elsewhere [26].

In the large pores ($H=40\sigma$), the densities of the coexisting phases were calculated in the temperature interval from $T=0.80$ to $T=1.15$ (T is scaled by ϵ/k_B, where k_B is a Boltzmann's constant). Totally 12 and 19 temperature points were studied for the pore with hard walls and weakly attractive walls, respectively. In the small pore ($H=12\sigma$) with hard walls, 45 temperature points (from $T=0.65$ to $T=1.13$) were studied. The lowest studied temperatures were close to (or even below) the bulk triple-point temperature of the studied LJ fluid [57], whereas the highest studied temperatures were only slightly below the respective pore critical temperatures.

The density profiles of the LJ liquid in pores were obtained by constant volume MC simulations, using the average densities of the liquid phase obtained in the GEMC simulations. The strong density gradient normal to the pore wall owing to the liquid-vapor interface detached from the wall makes the reliable determination of the density profiles very time consuming. This problem was partially overcome by using two kinds of moves in MC simulations. In addition to the standard MC moves with a maximal displacement of a molecule, which provides an acceptance probability of about 50%, we used long-distance molecular transfer inside the simulation cell: An attempt to place randomly chosen fluid molecule into randomly chosen position in the cell. The latter MC move is similar to the one used in GEMC simulations for molecular transfers between the two simulation boxes. Such long-distance molecular transfers essentially improve the sampling of density profiles. The local density was determined for layers of 0.02σ width and the resulting density profiles were averaged over 10^5 configurations taken each 1000th MC step. This yielded a statistical uncertainty less than 1%.

III. RESULTS AND DISCUSSIONS

The liquid-vapor coexistence curves, obtained for the pores with hard and weakly attractive walls, are shown in Fig. 1. The average number densities of the liquid and vapor phases (ρ_l and ρ_v, respectively) of a confined LJ fluid were calculated taking into account the volume accessible to the centers of molecules and scaled by σ^3. The pore critical densities we estimate as 0.23 ± 0.02 in both large pores and 0.26 ± 0.01 in small pore with hard walls. The pore critical temperatures we estimated as 1.164 ± 0.007 and 1.160 ± 0.013 for LJ fluid in pores with hard walls of width $H=40$ and 12σ, respectively and 1.177 ± 0.007 for the pore with $H=40\sigma$ and

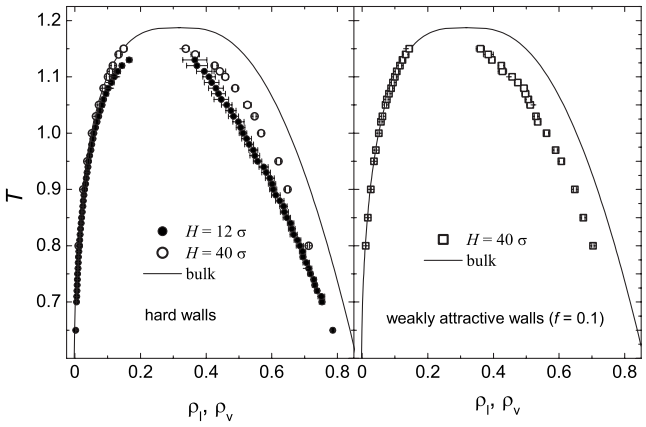

FIG. 1. Coexistence curves of the LJ fluid confined in the slit pores with hard and weakly attractive walls. The bulk coexistence curve of the LJ fluid [26] is shown by solid lines. ρ_l and ρ_v are the average densities of liquid and vapor phases in pores.

$f=0.1$. The bulk liquid-vapor coexistence curve of the same LJ fluid obtained by GEMC simulations [26] was found to be consistent with the bulk critical temperature $T_c=1.1876$ obtained using a histogram reweighting method with subsequent mixed-field finite size scaling [55]. The reduced temperature used below in the present paper $\tau=1-T/T_c$ measures the deviation of the temperature from this *bulk* critical temperature.

The density profiles $\rho_l(z,\tau)$ in the liquid phase of LJ fluid in three pores at all temperatures studied are shown in Figs. 2–4. For clarity, the simulated data points on these figures were smoothed by running average over 10 points. In a wide temperature range, which almost covers interval from freezing temperature to T_c, the liquid profiles $\rho_l(z,\tau)$ show gradual decrease approaching to the pore wall. This behavior is distorted in the narrow interval near the hard wall, where the simulated density rapidly decreases. This artificial drop of a fluid density very close to the hard wall is caused by the finite value of the maximal displacement normal to the wall in the conventional MC move. For some temperatures, we have reduced this effect by the decrease of the maximal displacement normal to the wall, that, however, required much

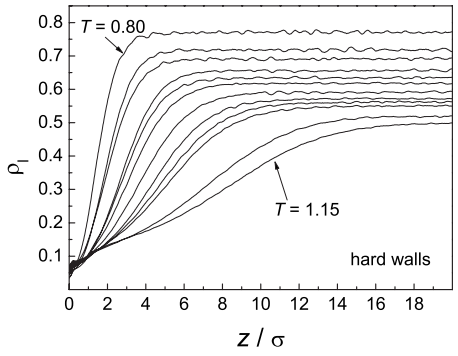

FIG. 2. Density profiles of the coexisting liquid phase of the LJ fluid confined in the slit pore of width $H=40\sigma$ with hard walls at all temperatures studied. The simulated data are smoothed by 10-point running average.

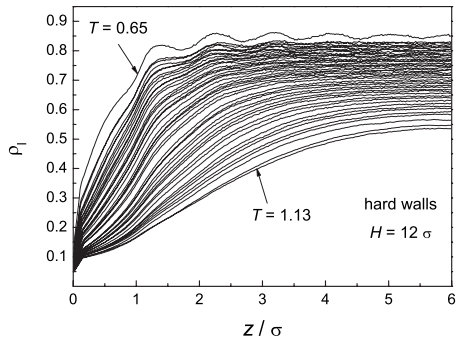

FIG. 3. Density profiles of the coexisting liquid phase of the LJ fluid confined in the slit pore of width $H=12\sigma$ with hard walls at 45 temperatures studied. The simulated data are smoothed by 10-point running average.

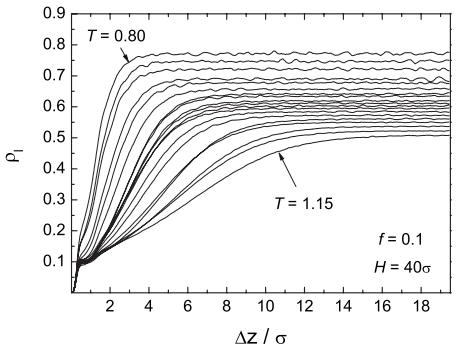

FIG. 4. Density profiles of the coexisting liquid phase of the LJ fluid confined in the slit pore of width $H=40\sigma$ with weakly attractive walls at all temperatures studied. The simulated data are smoothed by 10-point running average.

longer simulation runs to get adequate sampling of the density distribution. In the present paper we intend to establish the general laws which describe the liquid density profiles and which should not be dependent on the simulation details and specific boundary conditions in the contact area. Therefore, we have excluded from the further analysis the data points in the range $z<1\sigma$ and $z<0.13\sigma$ in the case of large ($H=40\sigma$) and small ($H=12\sigma$) pores, respectively.

The liquid density profiles near a hard wall were fitted to the classical interfacial equation:

$$\rho_l(z,\tau) = \frac{\rho_l^0(\tau) - \rho_v^0(\tau)}{2} \tanh \frac{z - L_0}{2\xi} + \frac{\rho_l^0(\tau) + \rho_v^0(\tau)}{2}, \quad (8)$$

where L_0, ξ, ρ_l^0, and ρ_v^0 are the fitting parameters. We have found, that in both studied pores with hard walls, $\rho_l(z,\tau)$ is perfectly described by Eq. (8) at all studied temperatures. The values of the fitting parameters for the pore with $H=40\sigma$ and 12σ are given in Tables I and II, respectively. The fitting parameter ρ_l^0 may be considered as a liquid density in the pore interior. In the large pore, ρ_l^0 does not exceed the bulk liquid density ρ_l^b at the same temperature on more than 0.5 to 2%. In the small pore, ρ_l^0 noticeably exceeds ρ_l^b in the whole studied temperature range and this effect enhances with temperature (see the last column in Table II). The fitting parameter ρ_v^0 shows large fluctuations around zero for LJ fluid in the small pore at all temperatures studied. Therefore, the fitting values shown in Table II were obtained at the fixed value $\rho_v^0=0$. The similar behavior of ρ_v^0 was seen also in the large pore at low temperatures. In such cases, the value $\rho_v^0=0$ was fixed during the fits and it is shown in brackets in Table I.

Universality of the description of the liquid density profiles in the pores with hard walls by interfacial Eq. (8) can be illustrated by the master plots. For these purposes, the local density and the distance to the wall were normalized in a way which takes into account the temperature dependence of the fitting parameters L_0, ξ, ρ_l^0, and ρ_v^0. The normalized in

TABLE I. The values of the fitting parameters ξ, L_0, ρ_l^0, and ρ_v^0 in Eq. (8) when fitted to the liquid density profiles in the large pore of width $H=40\sigma$ at different temperatures T (reduced temperatures τ). Uncertainties of the fitting parameters correspond to the confidence level 95%. The values of ρ_l^b were obtained by direct GEMC simulations of the liquid-vapor equilibrium [26].

T	τ	ξ/σ ±0.01	L_0/σ ±0.01	ρ_v^0 ±0.0005	ρ_l^0 ±0.01%	ρ_l^b
0.80	0.326	0.549	1.455	(0)	0.770	0.769
0.90	0.242	0.683	1.912	(0)	0.718	0.717
0.95	0.200	0.782	1.969	(0)	0.691	0.684
1.00	0.158	0.928	2.71	0.015	0.656	0.651
1.03	0.133	1.011	2.77	0.017	0.635	0.628
1.05	0.116	1.117	3.05	0.024	0.618	0.613
1.08	0.091	1.306	3.63	0.038	0.592	0.590
1.10	0.074	1.466	4.28	0.051	0.572	0.568
1.11	0.065	1.644	4.66	0.056	0.563	0.558
1.12	0.057	1.765	4.97	0.061	0.551	0.547
1.14	0.040	2.353	6.97	0.082	0.525	0.524
1.15	0.032	2.762	7.97	0.090	0.508	0.502

TABLE II. The values of the fitting parameters ξ, L_0, and ρ_l^0 in Eq. (8) when fitted to the liquid density profiles in the pore of width $H=12\sigma$ (with the fixed value $\rho_v^0=0$). Uncertainties of the fitting parameters correspond to the confidence level 95%. The values of ρ_l^b were obtained by direct GEMC simulations of the liquid-vapor equilibrium [26].

T	τ	ξ/σ ±0.01	L_0/σ ±0.0005	ρ_l^0 ±0.01%	$\frac{\rho_l^0}{\rho_l^b}$
0.65	0.453	0.420	0.246	0.849	1.013
0.70	0.411	0.426	0.380	0.827	1.013
0.71	0.402	0.438	0.368	0.824	1.015
0.72	0.394	0.429	0.445	0.818	1.013
0.73	0.385	0.431	0.477	0.813	1.012
0.74	0.377	0.439	0.462	0.809	1.013
0.75	0.368	0.435	0.515	0.803	1.011
0.76	0.360	0.447	0.529	0.800	1.014
0.77	0.352	0.453	0.554	0.795	1.013
0.78	0.343	0.456	0.600	0.789	1.012
0.79	0.335	0.462	0.576	0.785	1.013
0.80	0.326	0.473	0.611	0.781	1.014
0.81	0.318	0.478	0.635	0.776	1.014
0.82	0.310	0.485	0.687	0.769	1.012
0.83	0.301	0.492	0.705	0.765	1.013
0.84	0.293	0.505	0.706	0.762	1.016
0.85	0.284	0.509	0.756	0.755	1.014
0.86	0.276	0.515	0.783	0.750	1.015
0.87	0.267	0.526	0.773	0.746	1.017
0.88	0.259	0.534	0.826	0.740	1.016
0.89	0.251	0.548	0.891	0.734	1.016
0.90	0.242	0.556	0.924	0.729	1.017
0.91	0.234	0.562	0.912	0.724	1.018
0.92	0.225	0.575	0.929	0.718	1.018
0.93	0.217	0.591	0.990	0.713	1.020
0.94	0.208	0.603	1.009	0.707	1.021
0.95	0.200	0.625	1.122	0.699	1.018
0.96	0.192	0.646	1.230	0.693	1.019
0.97	0.183	0.651	1.144	0.687	1.020
0.98	0.175	0.670	1.211	0.680	1.020
0.99	0.166	0.690	1.240	0.675	1.023
1.00	0.158	0.706	1.287	0.668	1.023
1.01	0.150	0.726	1.318	0.663	1.027
1.02	0.141	0.742	1.326	0.656	1.028
1.03	0.133	0.767	1.402	0.647	1.027
1.04	0.124	0.795	1.432	0.642	1.032
1.05	0.116	0.811	1.496	0.633	1.031
1.06	0.107	0.852	1.589	0.624	1.031
1.07	0.099	0.884	1.612	0.617	1.035
1.08	0.091	0.899	1.643	0.610	1.040
1.09	0.082	0.949	1.690	0.600	1.040
1.10	0.074	0.964	1.724	0.593	1.047
1.11	0.065	0.965	1.752	0.575	1.036
1.12	0.057	1.042	1.881	0.561	1.033
1.13	0.049	1.075	1.883	0.552	1.042

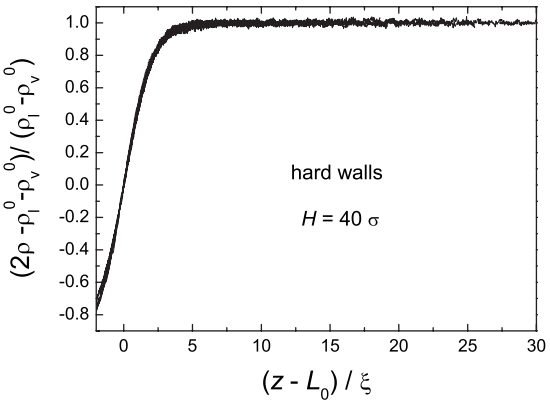

FIG. 5. Master plot of the 12 liquid density profiles $\rho_l(z,\tau)$ in the pore of width $H=40\sigma$ with hard walls. The parameters ρ_l^0, ρ_v^0, ξ, and L_0 where obtained from the fits of $\rho_l(z,\tau)$ to Eq. (8) and are shown in Table I. Thick dashed line represents the function $y=\tanh(x/2)$.

such a way density profiles at various temperatures should collapse on a single master curve. The master curves, obtained for the liquid density profiles in the pores with $H=40\sigma$ and $H=12\sigma$ are shown in Figs. 5 and 6, respectively (contrary to Figs. 2 and 3, simulated data are shown without smoothing). These figures evidence almost perfect description of the liquid density profiles by Eq. (8) in the temperature interval, which practically extends from freezing temperature to T_c.

The results of the fits of Eq. (8) to the density profiles of a liquid near a weakly attractive wall with $f=0.1$ are shown in Table III [in this case we used Δz instead of z in Eq. (8)]. The master curve in Fig. 7 evidences a perfect description of $\rho_l(\Delta z,\tau)$ (simulated data are shown without smoothing). Similarly to the case of a hard wall, the fitting parameter ρ_v^0 was found to be close to zero at low temperatures and the value $\rho_v^0=0$ was fixed during the fits in such cases (shown in brackets in Tables III). At $T>1$, the fitting values of ρ_v^0 increases with temperature, however, they are always signifi-

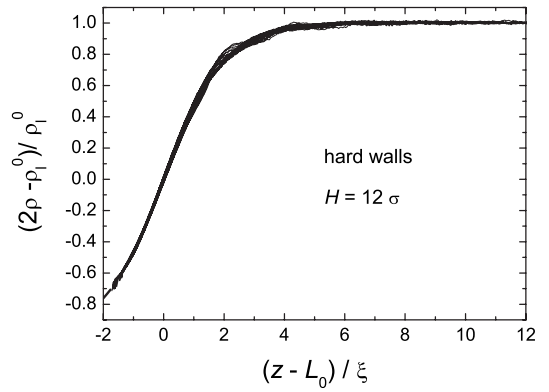

FIG. 6. Master plot of the 44 (from $T=0.7$ to 1.13) liquid density profiles $\rho_l(z,\tau)$ in the pore of width $H=12\sigma$ with hard walls. The parameters ρ_l^0, ξ, and L_0 where obtained from the fits of $\rho_l(z,\tau)$ to Eq. (8) and are shown in Table II. Thick dashed line represents the function $y=\tanh(x/2)$.

TABLE III. The values of the fitting parameters ξ, L_0, ρ_v^0, and ρ_l^0 in Eq. (8) when fitted to the liquid density profiles in the pore of width $H=40\sigma$ with weakly attractive walls ($f=0.1$) at different temperatures T (reduced temperatures τ). Uncertainties of the fitting parameters correspond to the confidence level 95%. The values of ρ_v^b and ρ_l^b were obtained by direct GEMC simulations of the liquid-vapor equilibrium in the bulk [26].

T	τ	ξ/σ ±0.01	L_0/σ ±0.01	ρ_v^0 ±0.001	ρ_l^0 ±0.01%	ρ_v^b	ρ_l^b
0.80	0.326	0.524	1.126	(0)	0.771	0.0098	0.769
0.85	0.284	0.589	1.303	(0)	0.746	0.0163	0.743
0.90	0.242	0.631	1.375	(0)	0.721	0.025	0.717
0.95	0.200	0.749	1.753	(0)	0.690	0.036	0.684
0.97	0.183	0.840	1.883	(0)	0.677	0.041	0.672
1.00	0.158	0.930	2.240	(0)	0.657	0.050	0.651
1.02	0.141	1.006	2.78	0.016	0.642	0.058	0.637
1.03	0.133	1.021	2.76	0.020	0.634	0.062	0.628
1.05	0.116	1.115	2.92	0.022	0.619	0.070	0.613
1.06	0.107	1.149	2.88	0.021	0.612	0.075	0.605
1.07	0.099	1.194	2.95	0.022	0.603	0.080	0.597
1.08	0.091	1.244	2.82	0.016	0.595	0.086	0.590
1.09	0.082	1.347	3.26	0.029	0.585	0.092	0.576
1.10	0.074	1.418	3.62	0.041	0.573	0.099	0.568
1.11	0.065	1.615	4.59	0.059	0.562	0.106	0.558
1.12	0.057	1.686	4.33	0.054	0.551	0.114	0.547
1.13	0.049	1.982	5.23	0.064	0.539	0.124	0.529
1.14	0.041	2.119	5.24	0.065	0.525	0.134	0.524
1.15	0.032	2.487	5.98	0.071	0.513	0.147	0.502

cantly smaller than the density of a saturated bulk vapor ρ_v^b at the same temperature (see Table III). This reflects depletion of a fluid density near the wall due to the missing neighbor effect. The values ρ_v^0 should be close to the saturated vapor density of bulk fluid ρ_v^b, when the liquid-vapor interface is far from the surface. However, this is not the case even for a fluid in the large pore with hard walls, where ρ_v^0 is also noticeably below ρ_v^b (see Table I). This difference is more pronounced for fluid in the pore with weakly attractive walls, where the interface should be located at some finite distance to the wall even in semi-infinite system.

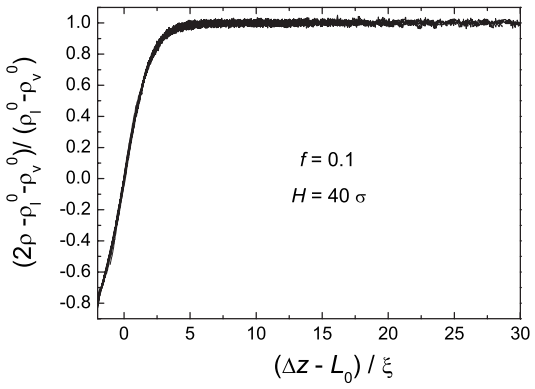

FIG. 7. Master plot of the 19 liquid density profiles $\rho_l(z,\tau)$ in the pore of width $H=40\sigma$ with weakly attractive walls ($f=0.1$). The parameters ρ_l^0, ρ_v^0, ξ, and L_0 where obtained from the fits of $\rho_l(z,\tau)$ to Eq. (8) and are shown in Table III. Thick dashed line represents the function $y=\tanh(x/2)$.

Long-range fluid-wall potential should cause power decay of a fluid density when moving away from the wall [5]. For the considered case of LJ fluid in the pore with weakly attractive wall ($f=0.1$), this may affect the interfacial-like profile, described by Eq. (8). For LJ fluid in the pore with three times stronger fluid -wall interaction ($f=0.3$), the interplay between the density depletion toward the wall and long-range fluid-wall attraction results in the appearance of a fluid density maximum both in a vapor [50] and in a liquid [49] phases. Careful analysis of the long-distance behavior of the liquid density profiles in the pore with $f=0.1$ shows that they remain convex up till the pore center at all temperatures studied. Similar monotonous density profile was obtained in the same pore at the bulk critical temperature [58].

The thickness L_0 of a drying layer strongly increases with temperature in all pores studied. The character of this dependence may be analyzed by using double logarithmic plot L_0 vs τ. The power law behavior of $L_0(\tau)$ in large pores with hard and weakly attractive walls with $f=0.1$ is clearly seen from Fig. 8. For the pore with hard walls, fit of $L_0(\tau)$ to the power law

$$L_0 \sim \tau^{-x} \tag{9}$$

gives $x=0.70\pm0.03$. Even better description of L_0 data is obtained using Eq. (4), assuming the shift $\delta\mu$ due to the

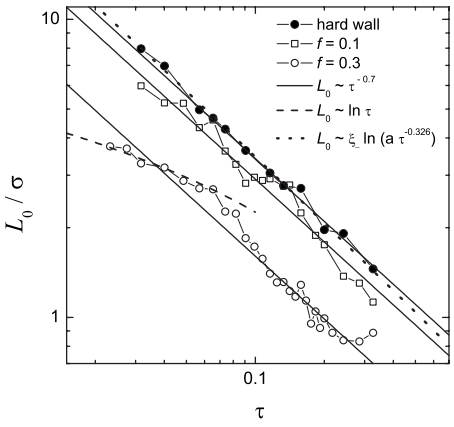

FIG. 8. Temperature dependence of the thickness L_0 of a drying layer near hard wall (solid symbols) and near weakly attractive walls: $f=0.1$ (open squares) and $f=0.3$ (open circles) [49] in pores of width $H=40\sigma$ obtained from the fits of $\rho_l(z,\tau)$ to Eq. (8).

confinement to be temperature independent (see dotted line in Fig. 8). Indeed, with approaching the critical point in semi-infinite system, L_0 should diverge stronger than the bulk correlation length due to vanishing of the order parameter $(\rho_l^0-\rho_v^0)$ with increasing temperature [see Eq. (4)].

In the pore with weakly attractive walls ($f=0.1$), the exponent x of the power law (9) can not be accurately estimated due to the scatter of the data points. Its power law behavior may be consistent both with some value of x close to 0.7 or with $x=\nu\approx 0.63$. The thickness of a drying layer in the pore with more attractive walls ($f=0.3$) is also shown in Fig. 8 for comparison. In the latter case, the power-law temperature dependence of L_0 is seen at low temperatures only. At higher temperatures ($\tau<0.06$) a weak logarithmic growth of L_0 follows the equation [49]:

$$L_0 = \ln(\tau^{-1}) + \text{const}, \tag{10}$$

with const$\approx 0.05\sigma$. Figure 8 evidences strong effect of the fluid-wall interaction on the thickness of the drying layer and its temperature dependence. Whereas weakly attractive potential ($f=0.1$) causes only slight shrinkage of a drying layer with respect to the case of a hard wall, stronger potential ($f=0.3$) changes temperature evolution of the drying layer quantitatively.

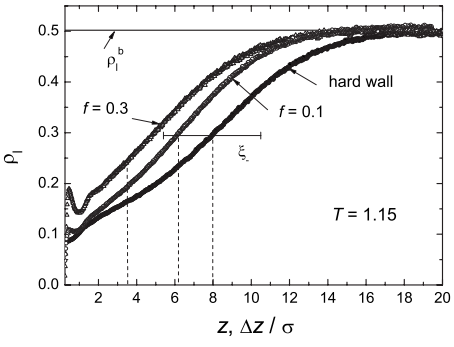

FIG. 9. Density profiles of the coexisting liquid phase ρ_l of the LJ fluid near hard wall and near weakly attractive walls with $f=0.1$ and 0.3 in the slit pores of width $H=40\sigma$ at $T=1.15$. The inflection points are indicated by the dashed lines. The bulk liquid density ρ_l^b is shown by solid line. ξ_- is the value of the bulk correlation length at this temperature.

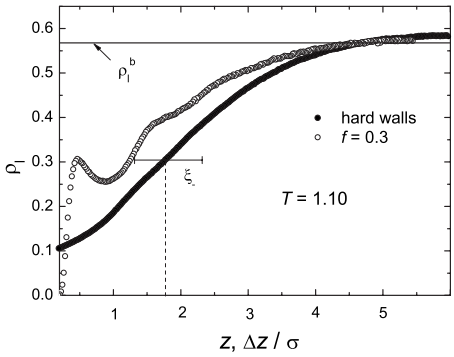

FIG. 10. Density profiles of the coexisting liquid phase ρ_l of the LJ fluid near the hard wall and near the weakly attractive wall with $f=0.3$ in the slit pores of width $H=12\sigma$ at $T=1.10$. The inflection point is indicated by the dashed line. The bulk liquid density ρ_l^b is shown by solid line. ξ_- is the value of the bulk correlation length at this temperature.

The liquid density profiles in pores with $H=40\sigma$ and different walls are compared directly in Fig. 9. Fluid-wall attraction shifts the inflection point of the interfacial-like liquid profiles toward the wall, and this shift increases with the strengthening fluid-wall interaction. In addition, an increase of the attractive interaction from $f=0.1$ to 0.3 seems to affect stronger the vapor branch of the interface and the fluid density strongly increases at the distances $\Delta z<L_0$ (see Fig. 9). Similar effects of the fluid-wall attraction on the drying layer are seen for LJ fluid in narrower pore with $H=12\sigma$ (see Fig. 10).

In order to investigate in more detail the effect of a fluid-wall interaction on the thickness of a drying layer, the liquid-vapor coexistence was simulated in the pore with $H=40\sigma$ and more attractive walls [$f=0.4$ in Eq. (7)] at $T=1.05$, 1.10, and 1.15. Dependence of L_0 on the interaction strength f at these 3 temperatures is shown in Fig. 11, where $f=0$ is assigned to the fluid-wall interaction in the case of a hard wall. Interestingly, that L_0 decreases roughly linearly with f at $T=1.05$ and 1.10. Both straight lines cross the x axis at about $f=0.64$. Behavior of L_0 at the highest temperature $T=1.15$ is also consistent with this approximately linear dependence on f, excluding the pore with hard walls, where thickness of a vapor layer is certainly larger than expected from the linear fit of L_0 for attractive potentials (upper straight line in Fig. 11). At all three temperatures studied, the drying layer disappears at $f\approx 0.64$. Note that the studies of the same LJ fluid at the bulk critical temperature yield roughly flat density profile, when $f=0.644$ [58]. This is a particular strength of the fluid-wall interaction, providing "neutral" wall condition, where neither drying nor wetting transition occurs near the wall.

The sharpness of the liquid-vapor interface is characterized by the parameter ξ in Eq. (8). In the absence of the capillary waves, the interface thickness is intrinsic and ξ is

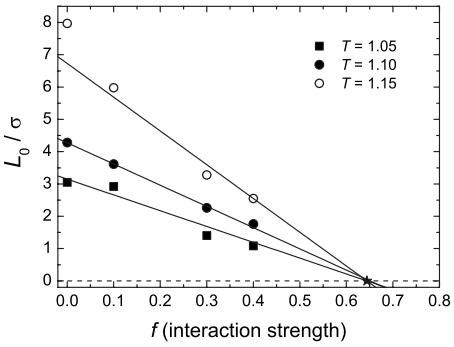

FIG. 11. Thickness L_0 of a drying layer as a function of the strength f of the fluid-wall interaction [Eq. (7)] at some temperatures T shown in the legend. The linear fits are shown by solid lines. The value $f=0$ is assigned to the hard wall. The value $f=0.644$ when $L_0 \approx 0$ is shown by star.

the bulk correlation length ξ_-. In the case of a free and infinite interface, the effective thickness of the liquid-vapor interface $\xi = \xi_-(1+k_BT/8\pi\gamma\xi_-^2)$ [31] may be significantly larger then the bulk correlation length due to the fluctuations of its position in direction normal to the interface. In general case, capillary waves may be expected at the liquid-vapor interface located far away from a hard wall. The long range fluid-wall interaction should suppress the capillary waves completely. In simulations, capillary waves may be effectively suppressed by the finite size of the simulated system in the lateral direction.

The values of the parameter ξ, obtained by fitting of Eq. (8) to the liquid density profiles in the large pores at various temperatures are shown in the upper panel of Fig. 12. The values of ξ obtained in the pores with hard walls and weakly attractive walls with $f=0.1$ practically coincide with the bulk correlation length ξ_- in a wide temperature range. Indeed, the temperature dependences of ξ well agree with the power law $\xi_- = \xi_0 \tau^{-\nu}$ with $\xi_0 = 0.29\sigma$ and $\nu = 0.63$, obtained for the bulk correlation length of the studied LJ fluid [26,49] (see solid line in Fig. 12). This is a strong indication, that the sharpness of the liquid-vapor interface in the large pores with hard walls and weakly attractive walls with $f=0.1$ is determined solely by the bulk correlation length ξ_-. Note that further increase of the fluid-wall interaction to $f=0.3$ results in a sharper liquid-vapor interface at low temperatures, which appears in ξ smaller than ξ_- (see open circles in Fig. 12).

The absence of the capillary waves near a wall with a long-range attraction is well understood theoretically (see review [5]). It is not very clear, why the interface is intrinsic in the pore with hard walls. In simulations, capillary waves near a hard wall may be suppressed first of all by the finite lateral size of the simulated system. To test this possibility, we have simulated a free liquid-vapor interface at the same temperatures keeping the same lateral size of the simulated system. Liquid phase was presented by a slab of width of 35 to 40σ placed near the middle of the simulation box, which width was adjusted to provide approximately equal volume fractions of liquid and vapor phases. The liquid and vapor densities far from interface were found indistinguishable from the respective bulk values obtained by GEMC simulations

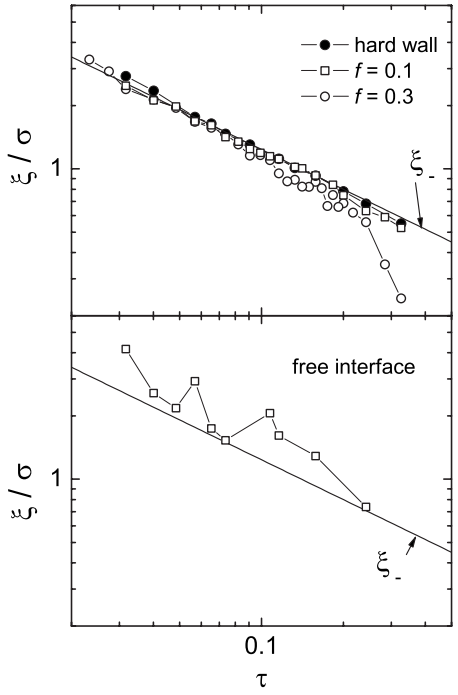

FIG. 12. Temperature dependence of ξ, which characterizes the sharpness of the liquid-vapor interface, in the pores of width $H=40\sigma$ with hard walls and weakly attractive walls with $f=0.1$ and 0.3 (upper panel) and for the free liquid-vapor interface (lower panel). The temperature dependence of the bulk correlation length $\xi_- = \xi_0 \tau^{-\nu}$ with $\xi_0 = 0.29\sigma$ and $\nu = 0.63$ is shown by solid lines.

[26]. The density gradient at the obtained free interfaces was perfectly described by Eq. (8) and the temperature dependence of ξ obtained from the fits is shown in the lower panel of Fig. 12. Obviously, the values of the parameter ξ, characterizing the sharpness of the liquid-vapor interface, exceeds the values of the bulk correlation length ξ_-. It is naturally to attribute this effect to the capillary waves which are not completely suppressed by the lateral size of the simulated system. The absence of capillary wave contribution at the liquid-vapor interface near the hard wall should be attributed to the proximity of the interface to the pore wall. So, the liquid-vapor interface is strongly affected by the proximity of the hard wall, at least up to the thickness of a drying layer of about 8σ.

The density profiles of the free liquid-vapor interface and interfaces near the hard wall in the large and small pores at $T=1.10$ are compared in Fig. 13. The similar comparison at the highest temperature studied $T=1.15$ is possible for the free interface and interface in a large pore of a width $H=40\sigma$ only (Fig. 14), as this temperature exceeds the pore critical temperature of the LJ fluid in small pore with hard walls. Obviously, the shape of the liquid-vapor interfaces near hard pore walls differs strongly from the profile of the free interface. The main difference is in the values of the parameter ρ_v^0 in Eq. (8). For a free liquid-vapor interface, ρ_v^0 is simply a density of the saturated vapor. Near a hard wall, fluid density is depleted due to the effect of a missing neighbor, which is unavoidable for a fluid near a boundary. As a result, the value ρ_v^0 for the interface near a hard wall is al-

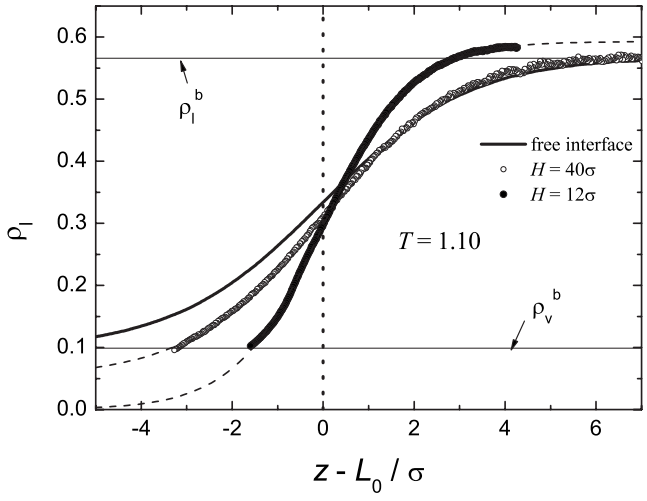

FIG. 13. Density profiles of the free liquid-vapor interface (solid line) and liquid density profiles near the hard wall at $T=1.10$ in large and small pores (symbols). Inflection points of all interfaces corresponding to $z-L_0=0$ are indicated by a vertical dotted line. The dashed lines show the fits of ρ_l to the Eq. (8).

ways below the density of the saturated vapor and this effect noticeably enhances with decreasing pore size.

Confinement affects drastically the density profile of a liquid phase. In small pore with hard walls, the density in the pore interior noticeably exceeds the bulk liquid density (see Fig. 15 and Table II), that reflects increase of the chemical potential with respect to its value at the bulk liquid-vapor coexistence. Decrease of the pore size from 40 to 12σ causes strong shrinkage of the drying layer. Besides, the temperature dependence of L_0 in the small pore with hard wall (closed circles in the upper panel of Fig. 16) differs strongly from the power law behavior, seen in the large pore (Fig. 8). At low temperatures ($\tau>0.2$), the thickness L_0 of the

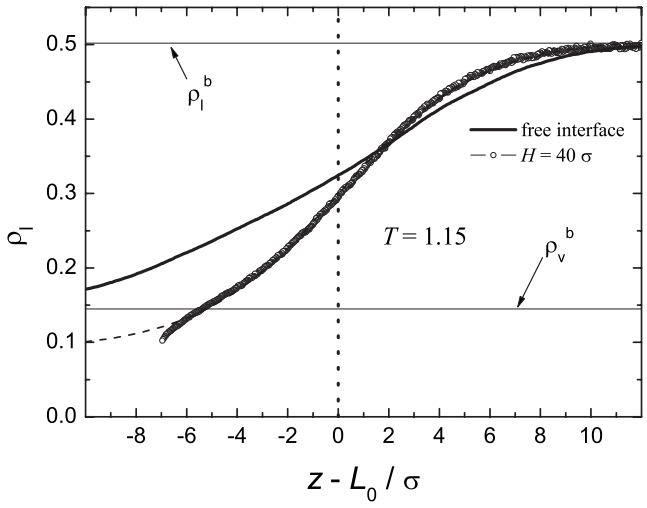

FIG. 14. Density profiles of the free liquid-vapor interface (solid line) and liquid density profiles near the hard wall in a large pore (symbols) at $T=1.15$. Inflection points of two interfaces corresponding to $z-L_0=0$ are indicated by a vertical dotted line. The dashed lines show the fits of ρ_l to the Eq. (8).

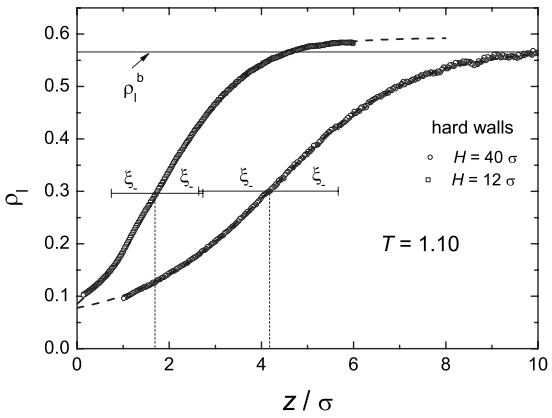

FIG. 15. Density profiles ρ_l of the liquid phase near the hard wall in two pores of different sizes at $T=1.10$. The density of bulk liquid ρ_l^b is shown by horizontal solid line. The fits of Eq. (8) to the profiles are shown by dashed lines. The inflection points are indicated by the vertical dotted lines.

drying layer follows the logarithmic law [Eq. (10)] with const$=-0.5\sigma$. This weak growth turns to the saturation, when L_0 exceeds 1σ and drying layer does not exceed 2σ at the pore coexistence curve. In the small pore of the same width with weakly attractive walls ($f=0.3$), the drying layer is almost completely bound to the wall at all temperatures and its effective thickness is close to 1σ (see open circles in Fig. 16).

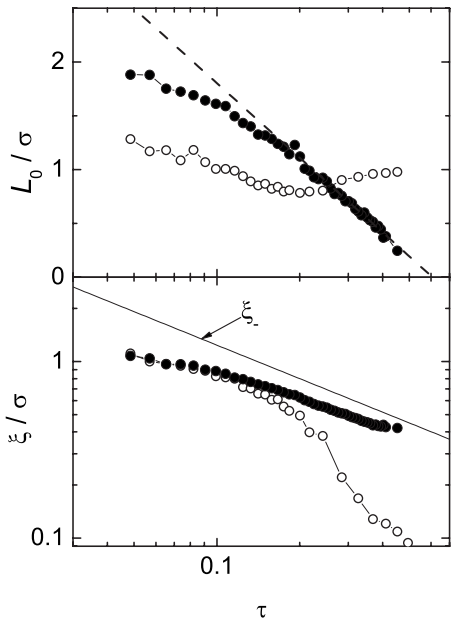

FIG. 16. Temperature dependence of the thickness L_0 of the drying layer and of the effective correlation length ξ near the hard wall (solid circles) and near the weakly attractive wall with $f=0.3$ (open circles [49]) in pores of width $H=12\sigma$ obtained from the fits of Eq. (8) to $\rho_l(z,\tau)$. The logarithmic divergence (10) with const$=-0.5\sigma$ is shown by dashed line. The temperature dependence of the bulk correlation length $\xi_-=\xi_0\tau^{-\nu}$ with $\nu=0.63$ and $\xi_0=0.29\sigma$ is shown by solid line.

The interface between the liquid and the drying layer is sharper in small pores, parameter ξ in Eq. (8) is noticeably below the bulk correlation length ξ_- (Fig. 16, lower panel). This difference increases with increasing temperature. The observed trend of ξ, together with the trend of L_0 to saturation, evidence the increasing importance of the confinement effect when approaching the critical temperature. Interestingly, the sharpness of the interface does not depend on the fluid-wall interaction at high temperatures (see Fig. 16, lower panel). So, ξ is determined mainly by the pore width and it should be equal to the correlation length in the bulk liquid whose chemical potential is equal to one of the liquid-vapor coexistence in pore.

IV. CONCLUSIONS

We have studied the temperature evolution of the drying layer of LJ liquid near weakly attractive wall along the pore coexistence curve. In all studied pores, liquid density profiles can be described by mean-field Eq. (8). In large pores, the sharpness of the interface is fully determined by the bulk correlation length. However, the vapor branch of the interface is strongly affected by the proximity to the solid boundary. Even when the interface is located at the distances 6 to 8σ from the wall, the missing neighbor effect causes noticeable depletion of a fluid density at the vapor branch of the interface. Such distortion prevents observation of the asymmetry in the shape of the liquid-vapor interface with respect to the interface position, which could be expected far away from the critical temperature. We have seen no capillary waves at the liquid-vapor interface near a hard wall. Comparison with the shape of a free liquid-vapor interface of the same lateral size shows, that this effect should be attributed to the proximity of the liquid-vapor interface to the interface between a hard wall and a vapor. The power-law decay of the liquid density caused by a long range attractive tail of a fluid-wall potential was not seen near the attractive wall with $f=0.1$. Note that in the case of a three time stronger fluid-wall potential ($f=0.3$) this effect causes appearance of a hardly distinguishable density maximum [50].

Our results for a LJ fluid in the pores with weakly attractive walls are consistent with a drying transition located at the bulk critical temperature. The drying transition is critical and the thickness of a drying layer near the wall with $f=0.1$ is proportional to the bulk correlation length, in accordance with theoretical expectations [9]. Near the surface with stronger fluid-wall interaction ($f=0.3$), power law behavior of L_0 is suppressed and the drying layer grows logarithmically when approaching the bulk critical temperature. We can not exclude, that this logarithmic growth crosses over to the power law behavior close to the critical temperature. Existence of the two distinct regimes in the temperature behavior of L_0, may reflect a first-order partial drying transition between thin and thick drying layers, expected with weakening the long-range fluid-wall interaction [11].

The thickness of a drying layer in the large pore with hard walls always exceeds the correlation length and the liquid-vapor interface may be considered as detached from the wall. Nevertheless, the proximity of the pore wall affects the vapor branch of the interface and stabilizes it against the capillary waves. The thickness of a drying layer near a hard wall increases with temperature slightly stronger than the bulk correlation length. Switching on of the arbitrary small long-range fluid-wall attraction suppresses drying layer, which disappears completely at some strength of a fluid-wall interaction, providing conditions of a "neutral" wall. Although a "neutral" wall interaction potential, in general, should depend on temperature, our data indicate that this dependence may be not strong.

Decrease of the pore size has strong impact on a drying layer and on the sharpness of a liquid-vapor interface. Due to the shift of the chemical potential of liquid-vapor coexistence in the considered small pores, the thickness of a drying layer is strongly suppressed and its temperature evolution changes qualitatively. In particular, even weak fluid-wall attraction makes interface in small pore completely bound to the wall. Strong confinement in small pore with hard walls results in only logarithmic growth of L_0, which turns to the saturation with increasing temperature.

The presented results indicate the possibility to describe the liquid density profiles near a weakly attractive walls by the analytical function [Eq. (8)], which contains just a few system-dependent parameters. It is important that both the thickness of a drying layer L_0 and the parameter ξ, determining the sharpness of a liquid-vapor interface, show rather universal temperature dependences. In particular, in large pores, the parameter ξ is a bulk correlation length, which may be estimated from the experimental or simulation studies of the bulk fluid. Besides, the dependence of L_0 on the strength of a fluid-wall interaction (Fig. 11) and dependences of L_0 and ξ on the pore size [49] are also may be described by simple empirical functions. This makes possible the prediction of the liquid density profiles along the liquid-vapor coexistence in various pores with weakly attractive walls.

ACKNOWLEDGMENT

Financial support from Deutsche Forschungsgemeinschaft (SPP 1155) is gratefully acknowledged.

[1] C. Ebner and W. F. Saam, Phys. Rev. Lett. **38**, 1486 (1977).
[2] J. W. Cahn, J. Chem. Phys. **66**, 3667 (1977).
[3] H. Nakanishi and M. E. Fisher, Phys. Rev. Lett. **49**, 1565 (1982).
[4] R. Pandit, M. Schick, and M. Wortis, Phys. Rev. B **26**, 5112 (1982).
[5] S. Dietrich, in *Phase Transitions and Critical Phenomena*, edited by C. Domb and J. L. Lebowitz (Academic Press, London, 1988), Vol. 12, pp. 1–217.
[6] E. Brezin, B. I. Halperin, and S. Leibler, Phys. Rev. Lett. **50**,

1387 (1983).
[7] R. Lipowsky, Phys. Rev. Lett. **52**, 1429 (1984).
[8] M. P. Nightingale, W. F. Saam, and M. Schick, Phys. Rev. B **30**, 3830 (1984).
[9] M. P. Nightingale and J. O. Indekeu, Phys. Rev. B **32**, 3364 (1985).
[10] C. Ebner and W. F. Saam, Phys. Rev. B **35**, 1822 (1987).
[11] C. Ebner and W. F. Saam, Phys. Rev. Lett. **58**, 587 (1987).
[12] A. O. Parry and R. Evans, Mol. Phys. **78**, 1527 (1993).
[13] A. O. Parry, J. Phys.: Condens. Matter **8**, 10761 (1996).
[14] P. Tarazona and R. Evans, Mol. Phys. **48**, 799 (1983).
[15] S. Dietrich and M. Schick, Phys. Rev. B **31**, 4718 (1985).
[16] M. J. P. Nijmeijer, C. Bruin, A. F. Bakker, and J. M. J. van Leeuwen, J. Phys.: Condens. Matter **4**, 15 (1992).
[17] G. B. Hess, M. J. Sabatini, and M. H. W. Chan, Phys. Rev. Lett. **78**, 1739 (1997).
[18] F. Ancilotto, S. Curtarolo, F. Toigo, and M. W. Cole, Phys. Rev. Lett. **87**, 206103 (2001).
[19] R. Steitz, T. Gutberlet, T. Hauss, B. Klosgen, R. Krastev, S. Schemmel, A. Simonsen, and G. Findenegg, Langmuir **19**, 2409 (2003).
[20] D. Schwendel, T. Hayashi, R. Dahint, A. Pertsin, M. Grunze, R. Steitz, and F. Schreiber, Langmuir **19**, 2284 (2003).
[21] T. R. Jensen, M. Ostergaard Jensen, N. Reitzel, K. Balashev, G. H. Peters, K. Kjaer, and T. Bjornholm, Phys. Rev. Lett. **90**, 086101 (2003).
[22] M. Maccarini, R. Steitz, M. Himmelhaus, J. Fick, S. Tatur, M. Wolff, M. Grunze, J. Janecek, and R. Netz, Langmuir **23**, 598 (2007).
[23] A. Poynor, L. Hong, I. K. Robinson, S. Granick, Z. Zhang, and P. A. Fenter, Phys. Rev. Lett. **97**, 266101 (2006).
[24] K. Binder, in *Phase Transitions and Critical Phenomena*, edited by C. Domb and J. L. Lebowitz (Academic Press, London, 1983), Vol. 8, pp. 1–144.
[25] I. Brovchenko, A. Geiger, and A. Oleinikova, J. Phys.: Condens. Matter **16**, S5345 (2004).
[26] I. Brovchenko, A. Geiger, and A. Oleinikova, Eur. Phys. J. B **44**, 345 (2005).
[27] W. T. Thomson, Philos. Mag. **42**, 448 (1871).
[28] M. E. Fisher and H. Nakanishi, J. Chem. Phys. **75**, 5857 (1981).
[29] H. Nakanishi and M. E. Fisher, J. Chem. Phys. **78**, 3279 (1983).
[30] F. van Swol and J. R. Henderson, Phys. Rev. Lett. **53**, 1376 (1984).
[31] R. Evans, J. R. Henderson, and R. Roth, J. Chem. Phys. **121**, 12074 (2004).
[32] F. F. Abraham, J. Chem. Phys. **68**, 3713 (1978).
[33] D. E. Sullivan, D. Levesque, and J. J. Weis, J. Chem. Phys. **72**, 1170 (1980).
[34] J. R. Henderson and F. van Swol, J. Chem. Phys. **89**, 5010 (1988).
[35] C. J. Segura, W. G. Chapman, and K. P. Shukla, Mol. Phys. **90**, 759 (1997).
[36] J. D. Weeks, K. Katsov, and K. Vollmayr, Phys. Rev. Lett. **81**, 4400 (1998).
[37] Y.-X. Yu and J. Wu, J. Chem. Phys. **116**, 7094 (2002).
[38] S. Zhou and A. Jamnik, Phys. Rev. E **73**, 011202 (2006).
[39] F. van Swol and J. R. Henderson, J. Chem. Soc., Faraday Trans. 2 **82**, 1685 (1986).
[40] F. van Swol and J. R. Henderson, Phys. Rev. A **40**, 2567 (1989).
[41] F. van Swol and J. R. Henderson, Phys. Rev. A **43**, 2932 (1991).
[42] J. H. Sikkenk, J. O. Indekeu, J. M. J. van Leeuwen, and E. O. Vossnack, Phys. Rev. Lett. **59**, 98 (1987).
[43] E. Velasco and P. Tarazona, J. Chem. Phys. **91**, 7916 (1989).
[44] M. J. P. Nijmeijer, C. Bruin, A. F. Bakker, and J. M. J. van Leeuwen, Phys. Rev. A **42**, 6052 (1990).
[45] M. J. P. Nijmeijer, C. Bruin, A. F. Bakker, and J. M. J. van Leeuwen, Phys. Rev. B **44**, 834 (1991).
[46] J. R. Henderson, P. Tarazona, F. van Swol, and E. Velasco, J. Chem. Phys. **96**, 4633 (1992).
[47] C. Bruin, M. J. P. Nijmeijer, and R. M. Crevecoeur, J. Chem. Phys. **102**, 7622 (1995).
[48] C. Bruin, Physica A **251**, 81 (1998).
[49] A. Oleinikova, I. Brovchenko, and A. Geiger, J. Phys.: Condens. Matter **17**, 7845 (2005).
[50] A. Oleinikova, I. Brovchenko, and A. Geiger, Eur. Phys. J. B **52**, 507 (2006).
[51] I. Brovchenko and A. Oleinikova, *Handbook of Theoretical and Computational Nanotechnology* (American Scientific Publishers, Stevenson Ranch, California, 2006), Vol. 9, Chap. 3, pp. 109–206.
[52] I. Brovchenko and A. Oleinikova, Mol. Phys. **104**, 22 (2006).
[53] I. Brovchenko, A. Geiger, and A. Oleinikova, Phys. Chem. Chem. Phys. **3**, 1567 (2001).
[54] I. Brovchenko, A. Geiger, and A. Oleinikova, J. Chem. Phys. **120**, 1958 (2004).
[55] N. B. Wilding, Phys. Rev. E **52**, 602 (1995).
[56] A. Z. Panagiotopoulos, Mol. Phys. **62**, 701 (1987).
[57] R. Agrawal and D. A. Kofke, Mol. Phys. **85**, 43 (1995).
[58] A. Maciolek, R. Evans, and N. B. Wilding, J. Chem. Phys. **119**, 8663 (2003).